Soil Dynamics and Earthquake Engineering 157 (2022) 107261

Contents lists available at ScienceDirect

Soil Dynamics and Earthquake Engineering

journal homepage: www.elsevier.com/locate/soildyn

Analysis of simplified time of liquefaction triggering methods by laboratory tests, physical modelling and numerical analysis

Sara Rios [a,*], Maxim Millen [b], Julieth Quintero [a], António Viana da Fonseca [a]

[a] Faculty of Engineering, University of Porto, Rua Dr. Roberto Frias, s/n, 4200-465, Porto, Portugal
[b] Department of Civil and Natural Resources Engineering, Faculty of Engineering, University of Canterbury, 20 Kirkwood Avenue, Ilam, Canterbury, 8041, New Zealand

ARTICLE INFO

Keywords:
Liquefaction
Centrifuge tests
Strain energy
FLAC numerical Analysis
Pore pressure

ABSTRACT

The damage resulting from earthquakes can result from the combination of seismic excitation and/or due to a build-up of excess pore pressure in the soil (liquefaction). These two effects are related since the reduction of soil stiffness due to a decrease in effective stress, modifies the seismic response of the soil deposit. Therefore, the expected level and type of damage is dependent on the amount of seismic energy reaching the ground surface before liquefaction. The development and validation of simplified liquefaction assessment methods to provide reasonable estimates of the build-up of excess pore pressure is essential for improving estimates of the level of seismic demand (ground shaking and permanent ground deformation) that may be experienced by a building. This paper presents two methods, one based on equivalent cyclic stress loading, and another based on the cumulative strain energy, which are used to predict the evolution of the pore pressure build up throughout time. The centrifuge tests performed in ISMGEO (Italy) during the LIQUEFACT project (www.liquefact.eu) were used as a benchmark to evaluate the predictive performance of the methods. Additionally, a series of one dimensional soil column effective stress and total stress analyses and single soil element simulations were run. Available laboratory tests were used to calibrate the parameters of the simplified methods, as well as input parameters for the numerical simulations. The results showed that both simplified methods had considerable bias. A direct comparison of the effective stress analyses, a set of effective stress analyses with limited drainage, and the centrifuge results, highlighted that the centrifuge experiments exhibited significant pore water flow that was not captured in the simplified models. Comparisons between the irregular loading in the one dimensional analyses compared to the uniform loading in the element tests highlighted shortfalls in the conversion from irregular to equivalent uniform loading. Comparisons between stress demands from total stress, effective stress and the simplified methods illustrated the limitations of relying on the total stress acceleration to estimate demands on a soil in a liquefying deposit.

1. Introduction

Soil liquefaction is a phenomenon in which the strength and stiffness of saturated, loose, frictional soils are significantly reduced by pore pressure build-up. Earthquake induced soil liquefaction may led to significant damage in structures and infrastructure founded on potentially liquefiable soils, as observed in Adapazari, Turkey, during the 1999 Kocaeli earthquake [1], in Christchurch, New Zealand ([2,3]), in Japan during the 2011 Tohuko earthquake [4] and more recently in the Croatian earthquake in 2020. The development of significant permanent ground deformation has been linked to the time of liquefaction triggering and in particular the post-liquefaction seismic energy [5]. Whereas numerous studies have shown that surface ground shaking reduces (at least high frequency content) after liquefaction has triggered [6]. Furthermore [7], have recently proposed a technique to stabilize a building in a liquefaction susceptible zone using a compact gravel layer immediately below the building, but leaving the underlying soil to liquefy, taking advantage of the dissipated energy due to liquefaction. However, complete liquefaction does not occur instantly at the beginning of shaking (e.g. Wildlife record from the 1987 Superstition Hills earthquake [8]), and therefore the building can be exposed to intense shaking prior to liquefaction or while the soil is in a semi-liquefied state.

Given the significant influence of excess pore pressure on building performance, it is essential to provide reasonable estimates of the likely

* Corresponding author.
E-mail addresses: sara.rios@fe.up.pt (S. Rios), maxim.millen@canterbury.ac.nz (M. Millen), julieth@fe.up.pt (J. Quintero), viana@fe.up.pt (A. Viana da Fonseca).

https://doi.org/10.1016/j.soildyn.2022.107261
Received 22 December 2021; Received in revised form 18 March 2022; Accepted 18 March 2022

build-up throughout the duration of shaking. Coupled, nonlinear effective stress numerical analyses are a good way to obtain that estimation but these approaches require the calibration of an important number of geotechnical parameters. Several simplified methods have been developed to estimate the factor of safety in relation to liquefaction triggering (e.g. Refs. [9,10]), however, these methods do not directly provide pore pressure build up throughout time. Recently, there have been three simplified methods: one stress based method from Ref. [5] which only provides an estimate of the time of triggering and other two that provide estimates of pore pressure build up throughout time. These latter methods are the stress based proposal from Ref. [11] and a strain energy method from Ref. [12]. The evaluation of these methods against field data is challenging, particular the stress-based methods, which require an estimate of the acceleration time series at the ground surface for total stress conditions (no pore pressure development). However, the use of centrifuge tests combined with numerical nonlinear time histories provide useful insights into the relative accuracy of these methods. Although it is recognized that centrifuge tests and time history analysis do not completely represent reality, the comparison of these methods to simplified procedures highlights where limits exist in the simplified procedures.

This work applies the two simplified estimates for pore pressure [11, 12] to predict the pore pressure build up and the seismic energy reaching the ground surface before liquefaction in a series of centrifuge tests. Additionally, 1D numerical analyses in FLAC2D® were performed and compared to the centrifuge results and simplified methods. The soil liquefaction resistance for each of the simplified methods and the numerical simulations was calibrated based on cyclic triaxial tests on the same soil.

2. Simplified methods to predict liquefaction

2.1. Background

The prediction of pore pressure has been extensively studied in the past decades due to its importance in triggering liquefaction and several simple empirical methods have been developed. These can be divided into three main groups: stress based, strain based and energy based. Stress-based methods were the first to be developed [13] resulting from observations made on stress-controlled cyclic triaxial tests where a uniform shear stress is applied measuring the build-up of pore pressure with increasing number of cycles. Although stress-based methods are widely used, there are some known shortfalls, particularly the reliance on the Palmer-Miner cumulative damage hypothesis, which assumes elastic or near elastic behaviour (quite contrary to the softening behaviour observed in liquefying soils) [14].

A strain based method was proposed by Ref. [15] from triaxial and simple shear tests, assuming that the residual pore pressure is a function of the accumulated shear strain. Ref. [16] also proposed a strain based method using the damage concept introduced by Ref. [17], which was then transformed into a stress based method by using the cyclic stress ratio (CSR) to define the damage parameter. This method was later improved by Ref. [18] and more recently by Ref. [19].

To minimize some limitations of the method based on equivalent cyclic stress, several energy based methods have been developed following the assumption made by Ref. [20] that pore water pressure generation can be uniquely related to the cumulative absolute strain energy or dissipated energy per unit volume ([12,21–23]). While dissipated energy refers to the area of stress-strain loops in a cyclic loading, the strain energy is the stored elastic potential energy at each load reversal. Integrating all the seismic spectra using variables such as the dissipated energy or the strain energy, these methods avoid:

- Instant parameters such as PGA, favouring cumulative seismic intensity measures (generally of less dispersion and allowing a full time series evaluation);
- the conversion to a uniform equivalent loading, since energy based methods are considered independent of the load amplitude.

A simplified dissipated energy-based liquefaction triggering procedure was proposed by Ref. [23] and recently updated in Ref. [24], as dissipated energy is closely linked to soil grain movement [25] and is a core aspect of numerous constitutive effective stress models (e.g. Ref. [26]). Dissipated energy has been demonstrated to be approximately constant across different amplitudes of loading and even for irregular loading histories [27]. However, methods that adopt dissipated energy have two major drawbacks. First, the estimation of the dissipated energy within a soil profile from a seismic shear wave is far from trivial as it is dependent on soil characteristics, particular the effective shear modulus, which changes as pore pressure increases. Secondly, the dissipated energy rapidly increases as the soil approaches liquefaction, and therefore a small change in the criteria for liquefaction triggering (e.g. change the limiting pore pressure ratio from 0.95 to 0.98), can have a large impact on the evaluated capacity.

2.2. Method based on the equivalent cyclic stress

[9] have provided a simple liquefaction triggering assessment method, where the factor of safety results from the ratio between the cyclic resistance ratio of the soil (CRR) and the cyclic stress ratio applied by the earthquake (CSR) defined as the ratio between the cyclic shear stress amplitude and the vertical effective stress at rest $\left(CSR = \frac{\tau}{\sigma'_{v0}}\right)$. In the procedure by Ref. [9] CSR is directly correlated to the peak ground acceleration (PGA) at the site assuming total stress conditions and a magnitude scaling factor adjusts the CSR to an equivalent number of cycles corresponding to a magnitude 7.5 earthquake. To convert the irregular cyclic loading provided by the earthquake into an equivalent uniform loading, a cyclic stress ratio of 0.65 of the maximum peak acceleration at the ground surface (PGA) was assumed, as indicated in equation (1):

$$CSR_{M=7,5} = 0.65 \cdot PGA \cdot \frac{\sigma_{v0}}{\sigma'_{v0}} r_d \frac{1}{MSF} \tag{1}$$

where σ_{v0} and σ'_{v0} represent, respectively, the total and effective stress at rest; r_d is the shear stress reduction factor, and MSF is the magnitude scaling factor.

In this work, a pore pressure method was used which requires the following: 1) a liquefaction resistance curve (LRC), 2) an estimate of the number of equivalent stress cycles throughout shaking, and 3) a relationship between number of cycles and pore pressure ratio.

The LRC can be defined using just two parameters, assuming a power law (equation (2)), where N is the number of cycles and a and b are soil dependent factors.

$$CRR = a \cdot N^{-b} \tag{2}$$

These two factors can be directly fitted to laboratory data, mainly cyclic triaxial tests or cyclic simple shear tests. Alternatively, CRR can be obtained by empirical correlations with in situ tests. In the case of equation (2), an empirical magnitude scaling factor (e.g. Ref. [9]) can be used to determine the slope parameter b using a relationship between magnitude and number of cycles (e.g. the relationships from Appendix A of [9] as explained in Ref. [28]). Once N_M and $N_{M=7.5}$ (number of cycles for a given magnitude, M, and magnitude 7.5 respectively) are determined then the parameter b can be determined from equation (3) for a given MSF.

$$\frac{N_A}{N_B} = \left(\frac{CSR_B}{CSR_A}\right)^{1/b} \Leftrightarrow MSF = \frac{CSR_M}{CSR_{M=7.5}} = \left(\frac{N_{M=7.5}}{N_M}\right)^{b} \tag{3}$$

The [13] cycle counting procedure (equation (4)) is used for the number of cycles based on the recorded surface total stress ground

motion and using a magnitude-based depth correction from Ref. [9].

The value for N_{ref} and the corresponding value of CRR_{ref} can be both taken from the LRC, typically taken at 15 cycles, which was the value that [29] indicates for the magnitude of 7.5. CSR_i corresponds to the normalized peak stress amplitude for each zero crossing of the CSR time series defined in equation (5).

$$\frac{N}{N_L} = \sum \left(\frac{CSR_i}{CRR_{ref}}\right)^{1/b} \cdot \frac{1}{2 \cdot N_{ref}} \tag{4}$$

$$CSR = |acc| \cdot \frac{\sigma_{v0}}{\sigma'_{v0}} \cdot r_d \tag{5}$$

where acc is the acceleration time series.

In expressions (1) and (5), r_d was calculated by equations (6)–(8) as a function of magnitude (M) and depth (z) using the expressions from Ref. [30]:

$$r_d = e^{[f(z)+g(z)\cdot M]} \tag{6}$$

$$f(z) = -1.012 - 1.126 \cdot sin\left(\frac{z}{11.73} + 5.133\right) \tag{7}$$

$$g(z) = 0.106 + 0.118 \cdot sin\left(\frac{z}{11.28} + 5.142\right) \tag{8}$$

To calculate the soil resistance, the CRR for 15 cycles to liquefaction (CRR_{15}) was corrected by the overburden correction factor (K_σ), defined by equation (9) from Ref. [9] where, C_σ is given by equation (10)

$$K_\sigma = 1 - C_\sigma ln\left(\frac{\sigma'_v}{P_a}\right) \leq 1.1 \tag{9}$$

$$C_\sigma = \frac{1}{37.3 - 8.27(q_{c1Ncs})^{0.264}} \leq 0.3 \tag{10}$$

In the evaluation of the centrifuge tests in this paper, a q_{c1Ncs} of 90 was used back calculated from a relative density of 50% (the density used in the centrifuge tests) using the following expression.

$$D_R = 0.465\left(\frac{q_{c1Ncs}}{0.9}\right)^{0.264} - 1.063 \tag{11}$$

Finally, the pore pressure versus number of cycles comes from Ref. [31] - equation (12).

$$r_u = \frac{2}{\pi} arcsin\left[\left(\frac{N}{N_L}\right)^{1/2\beta}\right] \tag{12}$$

where the pore pressure ratio (r_u) is defined as the ratio between the excess pore pressure generated and the vertical effective stress at rest, the N/N_L ratio is calculated by equation (4) and β is an empirical coefficient which can be determined by the following proposal of [32] – equation (13).

$$\beta = c_1 FC + c_2 Dr + c_3 CSR + c_4 \tag{13}$$

where FC is the soil fines content, Dr is the soil relative density and c_1, c_2, c_3 and c_4 are regression constants, which vary with the fines content. For FC<35%: $c_1 = 0.01166$; $c_2 = 0.007397$; $c_3 = 0.01034$; and $c_4 = 0.5058$; while for FC ≥ 35%: $c_1 = 0.002149$; $c_2 = -0.0009398$; $c_3 = 1.667$; and $c_4 = 0.4285$.

2.3. Method based on the cumulative strain energy

The method proposed by Ref. [12] is based on the cumulative strain energy (CASE, or NCASE when normalized by the vertical effective stress at rest) defined as the cumulative change in absolute strain energy. CASE can be represented as the sum of the absolute change in strain energy between the strain energy peaks in the response (equation (14)) where the average shear stress was obtained by equation (15), where τ is the shear stress and γ is the shear strain and j is the successive peak strain energy points.

$$CASE = \sum_{j=0}^{n_{peaks}} \left|\tau_{av.j}\right| \cdot \left|\gamma_{j+1} - \gamma_j\right| \tag{14}$$

$$\tau_{av.j} = \begin{cases} \dfrac{\left|\tau_{j+1} + \tau_j\right|}{2} & \tau_{j+1} \cdot \tau_j \geq 0 \\ \dfrac{\left|\tau_{j+1}^2 + \tau_j^2\right|}{2 \cdot \left|\tau_{j+1} - \tau_j\right|} & \tau_{j+1} \cdot \tau_j < 0 \end{cases} \tag{15}$$

In the estimation of the seismic demand, the NCASE demand at a certain depth ($NCASE_{z=h}$) (equation (16)) is approximated using the nodal surface energy spectrum (NSES) (equation (17)). $NCASE_{u,\xi=0}$ is the NCASE at a depth h, for a homogeneous linear soil deposit with zero damping; $\eta_{z=h}$ is a reduction factor to account for damping; and $G_{z=h}/G_{input}$ is the ratio of shear modulus at depth, h, compared to the shear modulus where the input ground motion is defined. $NCASE_{u,\xi=0}$ is computed with equation (17) as the cumulative change in absolute kinetic energy of the equivalent strain motion divided by the initial vertical effective stress, (σ'_{v0}) where $\dot{u}_{s,i}$ is the velocity of the equivalent strain motion at time, i, and ρ is the mass density. The equivalent strain motion is computed using equation (18) as the difference between the upward and downward motion at depth h, which is the same motion shifted by a time interval, Δt, corresponding to the travel time from h to the surface and back. The damping reduction factor, $\eta_{z=h}$, is the expected level of reduction in amplitude at depth h, due to damping, as computed in equation (19), where η_{total} is the ratio of the amplitude of the upward going wave at the surface compared to that at the base, and t_H is the travel time from the surface to the depth, h. Finally, η_{total} is calculated in equation (20), where ξ is the small strain damping, taken as the default of 0.03, and f_e is the energy frequency of the ground motion, with a default value of 2 Hz.

$$NCASE_{z=h} = \mathrm{NCASE}_{u,\xi=0} \cdot \eta_{z=h} \cdot \frac{G_{z=h}}{G_{input}} \tag{16}$$

$$NCASE_{u,\xi=0} = \frac{\rho}{\sigma'_{v0}} \cdot \sum_{i=1}^{n} \left|\Delta\left(\dot{u}_{s,i} \cdot \left|\dot{u}_{s,i}\right|\right)\right| \tag{17}$$

$$\ddot{u}_{s,i} = \ddot{u}_i - \ddot{u}_{i+\Delta t} \tag{18}$$

$$\eta_{z=h} = \eta_{total} + (1 - \eta_{total})/2 \cdot t_h / t_H \tag{19}$$

$$\eta_{total} = \exp(-\xi \cdot t_H \cdot 2 \cdot \pi \cdot f_e)^2 \tag{20}$$

For the application of this method to the prediction of pore pressure build up, a simple expression was proposed by Ref. [12], although it is recognized that this expression may depend on the type of soil:

$$r_{u,i} = \min\left(\sqrt{\frac{NCASE_i}{NCASE_{liq}}} \cdot r_{u,liq}; 1, 0\right) \tag{21}$$

where $NCASE_i$ corresponds to the NCASE demand that arrives to a given soil layer due to the seismic excitation and $r_{u,liq}$ corresponds to the pore pressure ratio at the time of liquefaction triggering, generally based on the double amplitude shear strain, the effective vertical stress or simply a pre-defined value of r_u (0.9, 0.95 or 0.98). $NCASE_{liq}$ corresponds to the NCASE necessary for soil liquefaction, being therefore a measure of soil resistance, such as CRR, with the additional advantage of being constant with stress amplitude but sensitive to soil properties.

3. Liquefaction resistance from laboratory tests

The resistance of the soil to liquefaction in terms of CRR_{15} and $NCASE_{liq}$ can be obtained by laboratory tests. The centrifuge tests

presented in the next section were performed with Ticino Sand, a well-known Italian sand extensively studied in the latest 40 years. It is a uniform medium to coarse sand, with angular and subrounded particles, composed by 30% Quartz, 65% Feldspar and 5% Mica [33] with the following index properties: $e_{min} = 0.574$, $e_{max} = 0.923$, $Gs = 2.68$, $D_{50} = 0.53$ mm and neglectable fines content. To evaluate the cyclic resistance of this sand the cyclic triaxial tests presented by Ref. [33] were used. Fig. 1 shows the CSR curves for Ticino Sand after converting the cyclic triaxial test data to simple shear data using the relation proposed by Ref. [33] based on a k_0 value of 0.44:

$$CSR^{SS} = 0.63 \times CSR^{tx} \quad (22)$$

The triggering limit for liquefaction was either 5% double amplitude shear strain or when the soil dropped below an effective vertical stress of 7 kPa (corresponding to $r_u = 0.93$) calculated as follows:

$$r_{u,liq} = \frac{\sigma'_v - \sigma'_{v,liq}}{\sigma'_v} \quad (23)$$

where $\sigma'_{v,liq}$ is 7 kPa.

Based on this data, equation (2) was adjusted using a b value of 0.34 as suggested by Ref. [29] for sand. This procedure returned CRR^{ss}_{15} equal to 0.097, 0.099 and 0.131 for relative densities of 49%, 54% and 57%, respectively. A value of $CRR^{ss}_{15} = 0.09$ was therefore taken to represent the soil in the centrifuge tests performed at a relative density close to 50%, which is similar to the value of $CRR^{tx}_{15} = 0.17$ obtained by Refs. [34,35] considering the triaxial test data not converted to simple shear. Therefore, the liquefaction resistance curve was established for $CRR^{ss}_{15} = 0.09$ and $b = 0.34$, and was used for the stress based method and to calibrate the PM4sand parameters used in the FLAC numerical analysis.

Note that for the calculation of β in the Stress based method (SBM) (equation (13)) zero fines content was assumed since Ticino Sand is a clean sand.

For the method based on the cumulative strain energy the soil resistance is measured by $NCASE_{liq}$, whose values were obtained from the [33] data. Fig. 2 shows the development of pore pressure versus

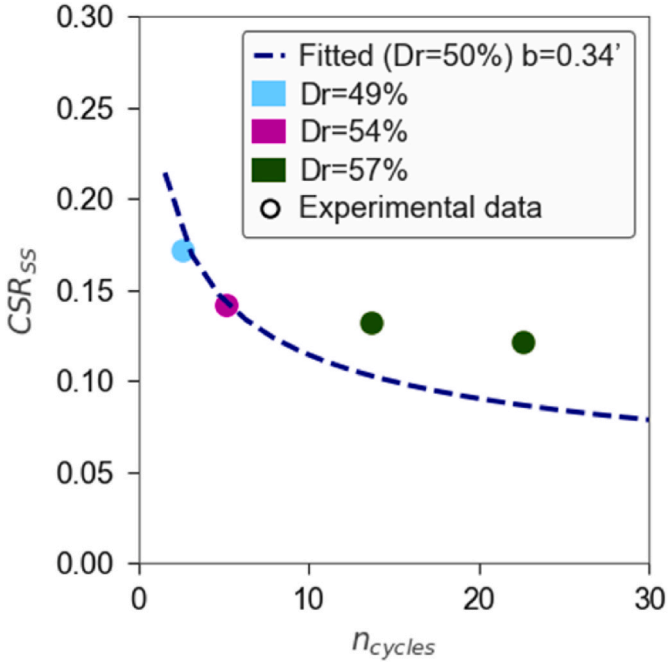

Fig. 1. Curves CSR versus number of cycles to liquefaction for a liquefaction criterion of 7 kPa of effective stress, where a trend line was adjusted with b = 0.34.

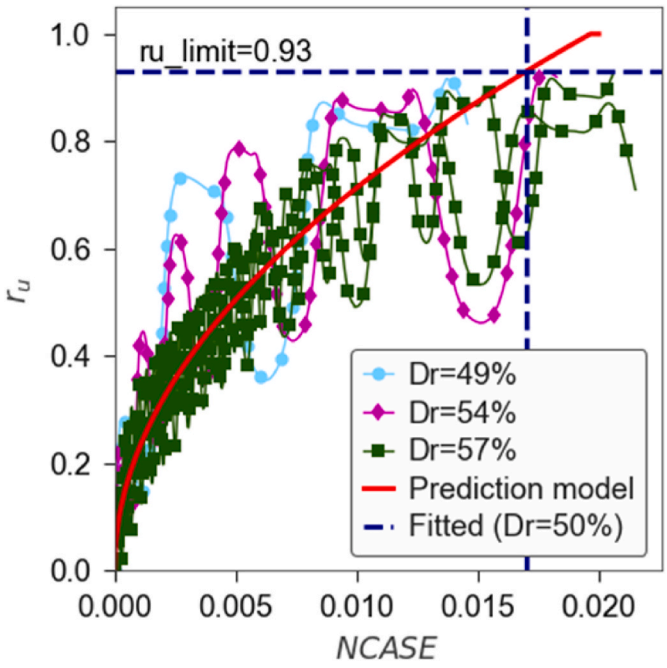

Fig. 2. Pore pressure development versus NCASE from the cyclic triaxial tests on Ticino Sand performed by Ref. [33] calculated for a liquefaction criterion corresponding to an effective stress of 7 kPa.

NCASE, where the square root function proposed by Ref. [12] was fitted to the data using a value of $NCASE_{liq}$ of 0.017. To compute the NCASE values from laboratory data, the axial strain (ε_a) was converted to shear strain (γ) using equation (24) valid for undrained conditions where Poisson's ratio can be assumed as 0.5 [36].

$$\gamma = 1.5 \cdot \varepsilon_a \quad (24)$$

4. Physical modelling

4.1. Description of the tests

The centrifuge tests analysed in this work were performed during LIQUEFACT project (www.liquefact.eu) at the ISMGEO laboratory (Instituto Sperimentale Modelli Geotecnici, in Italy). The soil profiles of the tested models had 15 m of homogeneous saturated loose sand sometimes topped by an overconsolidated clay layer, where different seismic excitations were applied.

The ISMGEO geotechnical centrifuge is a beam centrifuge with a 6 m diameter rotating arm, as explained in detail in Refs. [37,38]. The centrifuge is also equipped with a single degree of freedom shaking table fixed to the rotating arm, to simulate the seismic motion. In terms of model container, an Equivalent Shear Beam (ESB) box was selected instead of a laminar box [39]. The preparation of the sand layer comprised dry pluviation to the ESB container from a very small constant height around 3 cm, calibrated to obtain a relative density of 40% (which increases with the following procedures to around 50%). In some models, the top layer was made of Pontida clay, a low plasticity kaolinitic silty clay [40], previously overconsolidated in a consolidometer and then placed above the sand layer as described by Ref. [38].

The model was geometrically scaled down by a factor of N = 50 and the models were subjected to a centrifugal acceleration of 50g. In dynamic phenomena (as in excess pore pressure generation) the time scale factor is N while in consolidation/seepage phenomena (as in excess pore pressure dissipation) the time scale factor is N^2. To overcome this problem, the models were saturated with a fluid 50 times more viscous than water, using a solution of water and hydroxypropyl methylcellulose

(HPMC) at a concentration of 2%. Saturation was performed by creating a vertical seepage of the fluid until the volume of percolated fluid was at least equal to the estimated volume of voids in the soil.

The excitations simulated in these tests were based on representative earthquakes of Emilia Romana region in Italy where the LIQUEFACT project has performed a full scale earthquake simulation to induce liquefaction in free field conditions [41]. Different excitations were simulated to reproduce distinct levels of seismic intensity, depending on the return period considered (474, 975 and 2475 years), for a depth of 15 m (height of the model at prototype scale).

4.2. Data treatment

The raw data of the centrifuge tests results [42] were treated in order to convert the units from model to prototype. The scale factor to convert the model units to prototype was N = 50 according to the acceleration of the centrifuge. Table 1 summarizes the scaling ratios for the main parameters analysed. Since a fluid, more viscous than water, was used for the model saturation, a single scaling ratio was used for the time variable. This means, as indicated in Table 1, that 1 s in the model corresponds to 50 s in the prototype.

On the acceleration records, a 4th order Butterworth high pass filter of 0.1 Hz and a low pass filter of 20 Hz were used. The first aims at removing problems related with sensor inclination during the test and the second removes any high frequency noise related with the measurement device. The records were also cut to leave only the portion where shaking occurred together with 10 s before and 20 s after. As the record had a faint oscillating background acceleration, this trimming caused a bias acceleration at the start resulting in a non-zero average velocity. This was removed by calculating the acceleration, and then removing it over a 2 s window at the start of the record with an initial acceleration of zero. The data presented herein always refers to the prototype units converted as indicated above.

From the set of centrifuge tests performed in LIQUEFACT, a group was selected for being representative of free field conditions and without liquefaction mitigation measures such as drains or air injection devices. Table 2 summarizes the tests conditions of that selected group.

4.3. Data analysis

4.3.1. Seismic excitation

The generation of excess pore water pressure and liquefaction can dramatically change the dynamic response of a soil deposit due to the change in soil stiffness [8]. It is thus interesting to compare the energy arriving at the surface, using Arias Intensity, with the pore pressure build up inside the soil deposit. Arias Intensity [43] is an intensity measure related to the energy induced by the earthquake as defined in equation (25). It can incorporate the cumulative effects of ground motion duration and intensity on the response of structural and geotechnical systems [44] therefore a useful proxy for damage induced at the surface. Fig. 3 shows, for different depths, the Arias Intensity (Ia) time series (Fig. 3a), as well as the pore pressure ratio (Fig. 3b), and the base acceleration record (Fig. 3c). The centrifuge test selected for this comparison is a 15.5 m depth model with one layer of Ticino sand 14 m high topped by 1.5 m layer of Pontida clay where liquefaction develops at about 19 s (test 11 indicated in Table 2). Fig. 3a) shows that initially the rate of increase in Ia is similar for all depths, however, post-liquefaction,

Table 1
Scaling ratios of the main parameters analysed.

Parameter	*Model*	*Prototype*
Time (s)	t	t x N
Acceleration (m/s^2)	a	a/N
Stress (kPa)	σ	σ
Displacement (m)	d	d x N

Table 2
Conditions of the selected tests (ground motion properties from Ref. [39].

Test number	*Soil profile*	*GMID*	*PGA (g)*	*d_{90} (s)*	*$I_{A,max}$ (m/s)*
1	Ticino sand	17	0.215	15.09	0.348
2	Ticino sand	34	0.222	24.23	0.451
3	Ticino sand	31	0.198	18.63	0.601
10	Ticino sand + Pontida clay	34	0.222	24.23	0.451
11	Ticino sand + Pontida clay	31	0.243	21.76	0.673
15	Ticino sand + Pontida clay	31+	0.292	22.48	1.844

GMID = Ground motion ID; PGA = peak ground acceleration; d_{90} = duration calculated on the base of Arias Intensity; $I_{A,max}$ = maximum Arias Intensity.

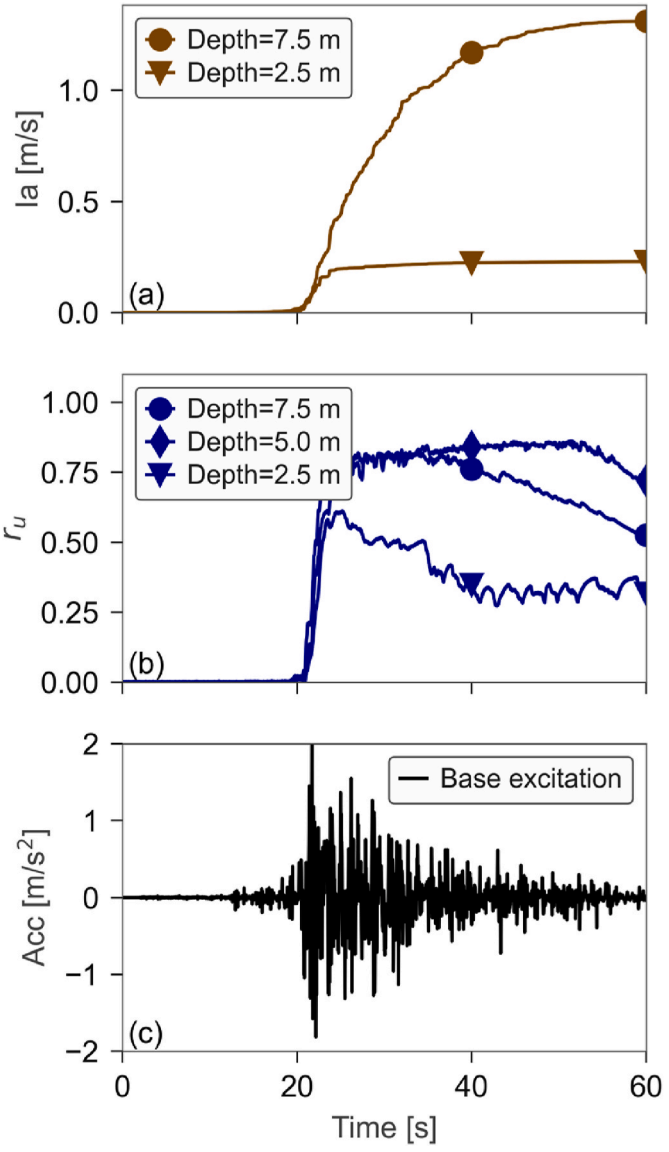

Fig. 3. Arias Intensity (a), pore pressure ratio (b) for different depths as well as corresponding base acceleration (c) – data from test 11 indicated in Table 2.

the energy arriving at shallower depths (2.5 m) is significantly lower than the one arriving at the bottom part of the sand layer (at 7.5 m deep). This means that liquefaction in the lower part of the deposit has reduced the demand arriving at the surface.

$$I_a = \frac{\pi}{2g}\int acc^2(t)\,dt \tag{25}$$

where acc is the acceleration time series and g is gravitation acceleration.

4.3.2. Ascending seepage

To understand whether the centrifuge tests suffered from seepage, the pore pressures measured in sensors positioned at different depths of the same vertical line were analysed. Test 11 used in the previous section 4.3.1 (Fig. 3) was also selected for this analysis. Fig. 4 show the excess pore pressure (Δu) evolution along the soil profile for the different time instants:

- 19 s: start of the seismic excitation (hydrostatic condition);
- 21.6 s: point of maximum acceleration;
- 24 s: start of maximum excess pore pressure;
- 45 s: point of high pore pressure ratio;
- 56 s: end of seismic excitation

From Fig. 4 for 21.6 and 24 s the change in excess pore pressure with depth is higher in the upper part of the model than in the lower part. This can be explained by ascending seepage in the model, which can be confirmed by calculating the hydraulic heads in the top and bottom. It is interesting that the hydraulic head loss given by the difference between those values is much higher than the vertical distance between the two points, indicating a hydraulic gradient higher than 1 (equation (26)). In this case the hydraulic gradient gave 2.1 m/m between the top and the base.

$$i = \frac{\Delta h}{l} = \frac{(u_{base} - u_{top}) + (y_{base} - y_{top})}{(y_{base} - y_{top})} \tag{26}$$

where u is the pressure and y is the point depth.

On the other hand, Fig. 4 show that at 56 s the excess pore pressure (and consequently the pore pressure ratio) has decreased on the lower part of the model but it is still high in the upper part, most likely due to the ascending seepage.

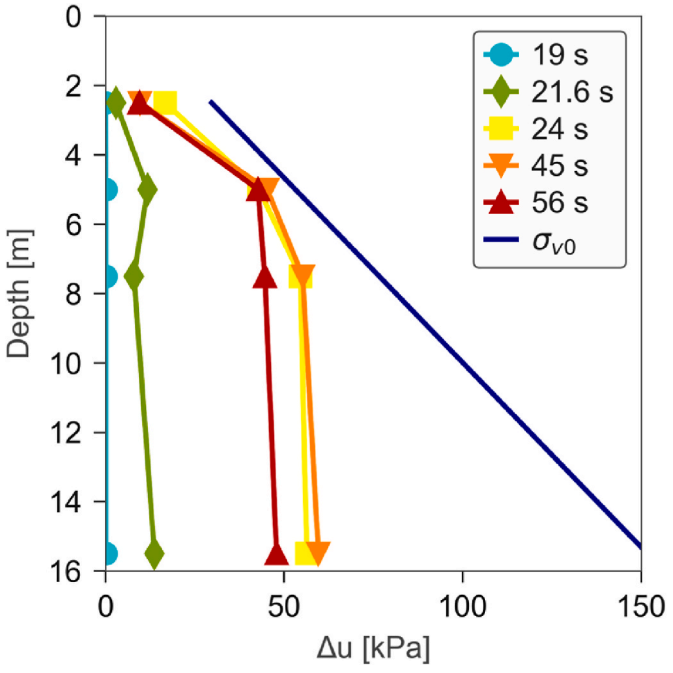

Fig. 4. Evolution of excess pore pressure, Δu, with depth for different time instants: 19 s, 21.6 s, 24 s, 45 s, and 56 s – data from test 11 indicated in Table 2.

5. Numerical analysis

5.1. Numerical element tests to calibrate constitutive parameters

As will be described in section 5.2, the centrifuge tests were numerically simulated using 1D analyses in FLAC2D®, a numerical modelling software for advanced geotechnical analysis of soil developed by Itasca Consulting Group Inc [45]. Within the LIQUEFACT project (www.liquefact.eu) a large effort has been dedicated to compare the performance of several constitutive models and different computational codes in predicting the experimental behaviour observed in these centrifuge models. Ref [46], for instance, compared the performance of three different constitutive models (PM4Sand, UBC3D-PLM and PDMY02) in terms of numerical prediction of the engineering demands parameters (e.g. $r_{u,max}$) measured in the centrifuge tests. Since these results show a good approximation between numerical and centrifuge tests results, PM4Sand [47] was used to simulate the liquefiable soils behaviour in this work. The parameters were calibrated using the laboratory tests described in section 3.

The PM4Sand is a sand plasticity model specially developed for geotechnical earthquake engineering applications following basically the framework of the stress-ratio controlled, critical state compatible, based on the bounding surface plasticity model for sand from Ref. [48] with modifications by Ref. [47] to improve its ability to approximate stress-strain responses pre and post liquefaction.

The calibration of PM4Sand was based on [33] having a relative density (Dr) of 50%, a maximum void ratio (e_{max}) and minimum void ratio (e_{min}) of 0.923 and 0.574 respectively.

Additionally, the shear modulus was considered stress dependent according to equation (27), where, G_0 was taken as 624 according to Ref. [34], p_{atm} is the atmospheric pressure and p' is the mean effective stress.

$$G = G_0 \cdot p_{atm} \cdot \sqrt{p'/p_{atm}} \tag{27}$$

The contraction rate parameter (h_{po}) was calibrated as 0.2, to best capture the fitted liquefaction resistance curve, as shown in Fig. 5 for r_u = 0.93 or double amplitude strain of 5%. The PM4sand parameters are summarised in Table 3 while all remaining secondary parameters were left at their default values.

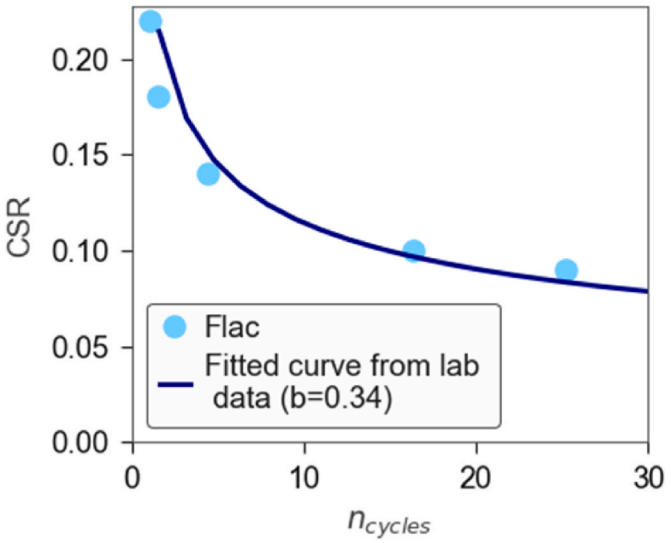

Fig. 5. Calibration of hpo parameter comparing element tests from FLAC and from laboratory.

Table 3
PM4sand parameters for Ticino sand.

Parameter	*Description*	*Value*
G_0	Shear modulus coefficient	624
h_{po}	Contraction rate parameter	0.2
p_a	Atmospheric pressure	101.3 kPa
e_{max}	Maximum void ratio	0.923
e_{min}	Minimum void ratio	0.574
ϕ'_{cv}	Critical state friction angle	34
υ	Poisson's ratio	0.3

5.2. Description of 1D numerical analysis

Nonlinear effective stress one dimensional analyses (ESA) were used to simulate the centrifuge test. The mesh consisted of a single column of zones, and laterally adjacent grid points were attached to move together in both horizontal and vertical displacements. The zones in each layer were sized to be equal or less than 0.5 m. The liquefiable Ticino sand was modelled with the PM4Sand model as indicated above in section 5.1. The non-liquefiable Pontida clay was modelled with the Mohr-Coulomb model and the hysteretic damping option, to match the expression from Ref. [49] for a plasticity index of 30. An additional 1.5% Rayleigh damping was specified at 0.2 Hz and 5Hz to mitigate numerical instability. The base of the soil profile was modelled as a rigid base to represent the base of the centrifuge box. The recorded base motions from the centrifuge tests were applied to the rigid base of the numerical analyses.

Additionally, nonlinear total stress analyses (NLTSA) were performed where the bulk modulus of the water was set to zero to avoid the build-up of pore pressure, whereas for the effective stress analyses it was set to 2.2 GPa.

The effective stress analysis were also repeated using a lower permeability for the liquefiable layer which was set to $k = 5 \times 10^{-5}$ m/s (ESA_low_k) which reduced the more extreme effects of drainage, while the benchmark analyses were performed with $k = 5 \times 10^{-4}$ m/s (ESA) to best match the water flow behaviour observed in the tests (consistent with permeability coefficient back calculated by Ref. [35] from these tests).

5.3. Comparison of 1D numerical analysis with centrifuge results

Fig. 6 shows a comparison of the simulated and centrifuge test surface accelerations for the same test 11 presented before. In terms of the seismic energy arriving at the surface, the non-linear effective stress analysis (ESA) and the non-linear total stress analysis (NLTSA) were compared to the acceleration measured at the surface in the centrifuge test. Fig. 6 shows a good agreement between measured and non-linear effective stress values indicating that the numerical model could reasonably capture the behaviour of the centrifuge test. The total stress analysis had higher spectral acceleration at low periods as a consequence of not having liquefaction.

The centrifuge data was compared to ESA in terms of the pore pressure ratio obtained at different heights in the model (Fig. 7), where a good agreement was observed except for the top sensor.

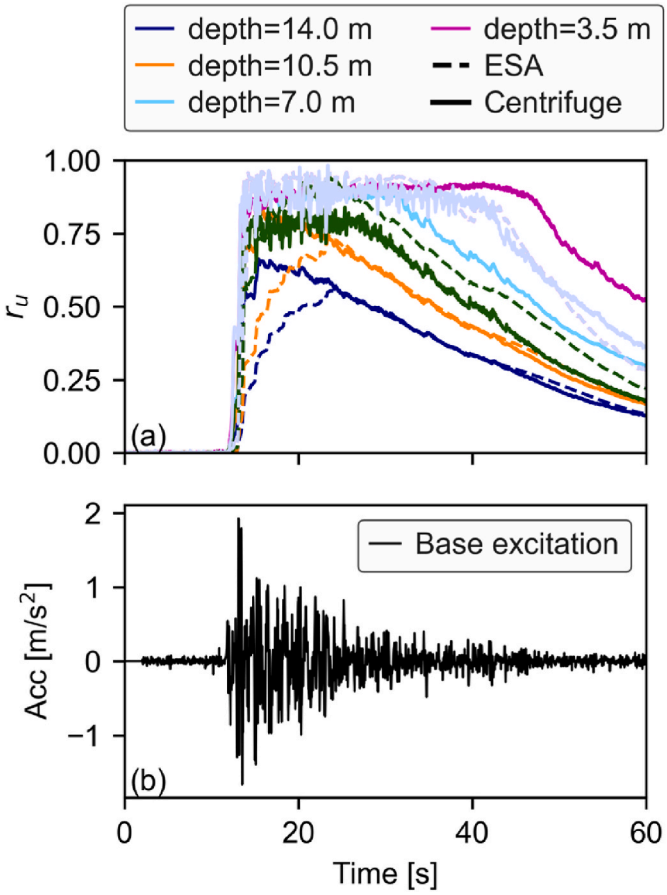

Fig. 7. a) Comparison of the pore pressure ratio evolution measured in the centrifuge test (solid lines) with the same values obtained in the ESA analysis (dashed lines); b) base seismic excitation – data from test 11 indicated in Table 2.

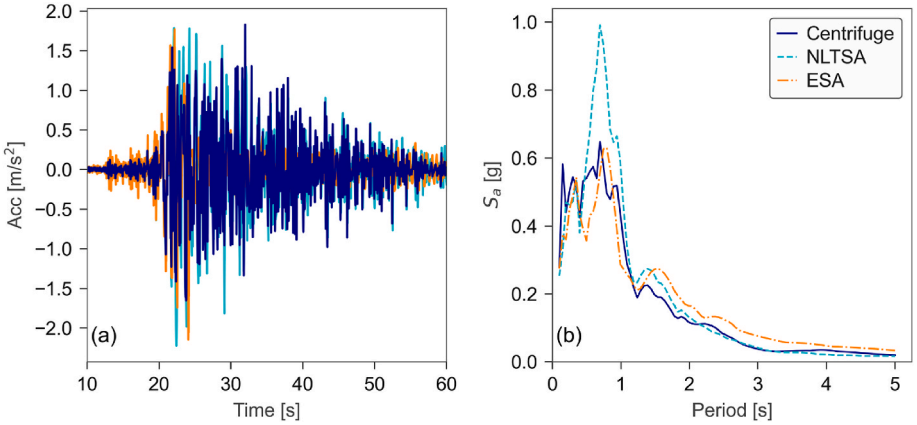

Fig. 6. Surface acceleration obtained in the numerical analysis (in total stresses – NLTSA and effective stress analysis – ESA) and in the centrifuge test in terms of acceleration time series (a) and spectral acceleration (b) – data from test 11 indicated in Table 2.

6. Comparison between simplified methods, centrifuge tests and numerical analysis

6.1. Input motions for the simplified methods

Since the simplified methods make use of an equivalent surface motion under total stress conditions (no pore pressure build up) but the centrifuge tests always considered pore pressure build up, the demand could not be directly determined. Instead the surface ground motion from the FLAC total stress analyses was used for computing the demands for the simplified methods. An alternative approach where the base motion was used to compute the demands was explored in Refs. [11,50]. However, this required the development of scale factors to account for the change in the location of the input motion, which had considerable uncertainty.

6.2. Comparison of liquefaction demand

To better understand the differences between the simplified methods, liquefaction demand in terms N/N_L ratio (for the stress based method – SBM described in section 2.2) and $NCASE/NCASE_{liq}$ (in terms of strain energy based method – SEBM – described in section 2.3) was computed with the corresponding simplified method and three sets of simulation results (ESA, ESA_low_k and NLTSA). Fig. 8a) presents the N/N_L ratio while Fig. 8b) the $NCASE/NCASE_{liq}$, both at a time of 24 s (on the precipice of liquefaction). At the surface, the SBM provided similar estimates to the NLTSA, whereas the SEBM differed substantially from the NLTSA results. In both graphs the NLTSA is quite different from ESA, especially at higher depths, due to soil softening and energy dissipation as a result of pore pressure build up. However, for NCASE the ESA demand is only less than the NLTSA demand below 6 m, while near the surface it is higher.

6.3. Comparison of pore pressure

Fig. 9 presents a comparison between pore pressure values measured in the centrifuge tests with the ones estimated by the simplified methods, together with the numerical analysis presented above. The same centrifuge test 11 used in section 5.3 was considered in this analysis. Fig. 9a) shows the sensor located in the upper part of the sand layer (at 5.0 m of depth), while Fig. 9b) shows r_u for the sensor placed in the middle of the liquefiable layer (at 7.5 m of depth). Although both simplified methods have different theoretical assumptions to estimate demand and capacity, they can provide reasonable estimates of pore pressure development.

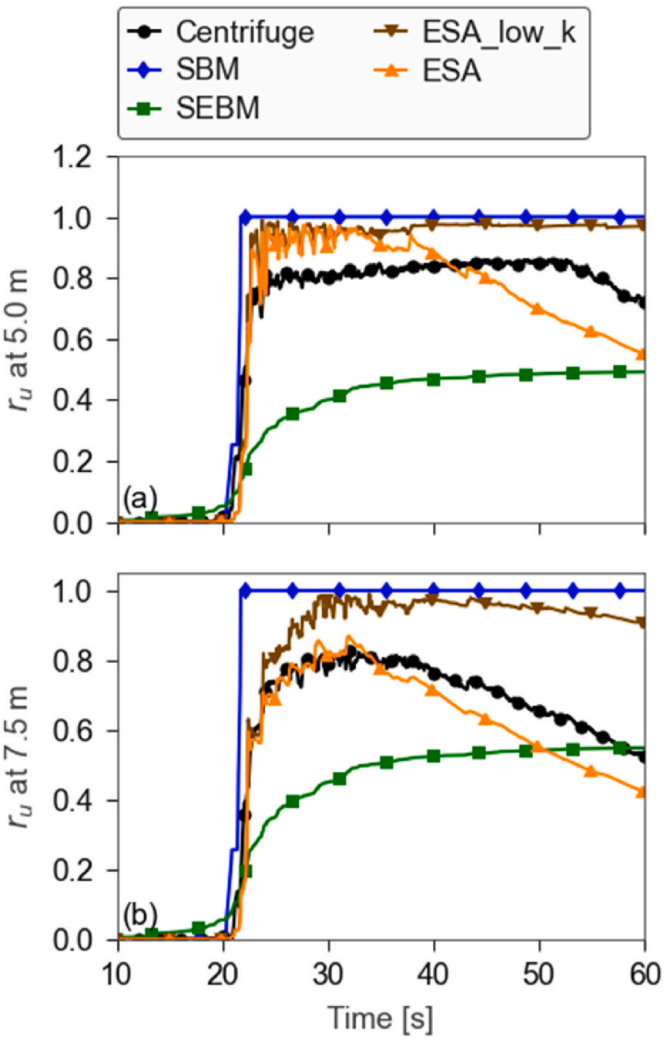

Fig. 9. Comparison of the pore pressure ratio evolution estimated by the simplified methods with the r_u values obtained in the centrifuge tests and numerical analysis for two different depths: a) at 5 m (upper zone of the sand layer); b) at 7.5 m (middle of liquefiable layer) – data from test 11 indicated in Table 2.

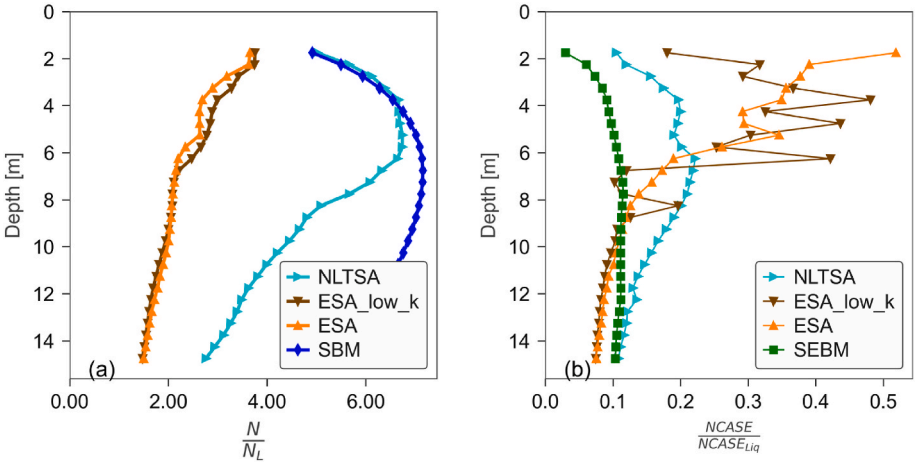

Fig. 8. N/N_L (a) and NCASE (b) profile with depth at 24 s obtained with different methods: Simplified method with surface motion obtained in FLAC NLTSA, ESA_low_k, ESA and NLTSA – data from test 11 indicated in Table 2.

As demonstrated above the system suffers from significant ascending seepage which can increase or decrease r_u depending on the hydraulic gradient, leading to some differences between real and estimated r_u values. This is demonstrated in Fig. 10 where the pore pressure is far greater at a depth of 4–8 m (region of greatest demand) for the low permeability analysis (ESA_low_k), compared to the ESA where pore pressures are more uniform due to drainage. Drainage can clearly have two significant effects, as high pore pressure flows to low pore pressure regions this causes an increase in pore pressure in the lower region beyond what is caused by the contraction of the soil in that region. Furthermore, the high pore pressure region may not reach full liquefaction if the rate of dissipation exceeds the rate of pore pressure build up due soil contraction. This is more evident in the cases where lower pore pressure values were observed in centrifuge tests (Fig. 10a).

7. Comparison of results

7.1. Sensors and parameters for comparison analysis

To facilitate a fair comparison between the simplified methods and the centrifuge tests only a subset of the pore pressure transducers were used. The sensors near the surface were excluded, due to difficulties in obtaining the capacity at very low confining stresses and sensors near the surface exhibited significant vertical water seepage as mentioned above. Additionally, sensors located in the clay layer or that did not register pore pressure due to technical problems were excluded. This selection resulted in 21 sensors that were used in the following analysis.

8. Results

A comparison of all 21 selected sensors was performed to evaluate the performance of the two prediction models. Since many tests did not reach liquefaction, and others suffered from rapid drainage, the evaluation was split into two categories. Category A consisted of all sensors where $r_u > 0.7$ (10 sensors), and Category B contained the remainder (11 sensors). In Category A the amount of seismic energy (Arias Intensity) released at the base motion sensor before reaching $r_u = 0.7$ was compared between the centrifuge and the two models (example shown in Fig. 11a). Input Arias intensity at $r_u = 0.7$ was considered an indicative proxy for a comparison between the estimated and actual amount of energy reaching the surface at that point, rather than using the absolute time which contains an arbitrary length of no shaking at the start. For Category B, the maximum r_u value from the centrifuge test is compared against the r_u from each model at the same time instance (example shown in Fig. 11b).

Fig. 12 presents the comparison of the centrifuge tests with the simplified methods, for the two categories identified above, respectively in Fig. 12a) for the cases where the sensor $r_u > 0.7$, and in Fig. 12b) for the cases where the sensor $r_u < 0.7$. It becomes clear from the graphs that the SBM (blue colour) tends to over predict pore pressure build up while the SEBM (green colour) tends to underpredict. SBM correctly estimates liquefaction in most cases, but it tends to predict liquefaction in cases where it does not happen. The opposite occurs for the SEBM.

A comparison of the ESA results (orange colour) versus the centrifuge results shows a reasonable match, with all results except one predicting the pore pressure ratio or Ia within the 1:2 and 2:1 bounds. In evaluating the observed errors, it should be noted that in many cases pore pressure builds up rapidly over less than 3 s with a large release of Ia, and therefore small errors in time result in significant changes to the Ia reported in the model (Fig. 12a). Whereas for Category B, peak pore pressure is probably affected by drainage, as indicated by the difference between ESA and ESA_low_k (brown colour) results, where in many cases, ESA_low_k tended to reach slightly higher r_u values since the lower permeability prevented the dissipation of pore pressure.

To better understand the results and provide insights into how the simplified methods can be improved, the following two sections evaluate the assumptions of each method against the FLAC results.

8.1. Evaluation of assumptions of the stress based method

The different assumptions of the simplified stress based method as outlined below were evaluated based on the results of test 11 using Figs. 8a), 9 and 13a):

I. Assumption: *The total stress cyclic stress demand can be approximated using the surface acceleration and a rigid body assumption with a correction (r_d factor) for deformation.* From Fig. 8a), a comparison of the number of cycles computed using the surface acceleration with the correction for deformation (denoted as SBM in the figure) provided an excellent match to the NLTSA for the top 6 m and then overpredicts at greater depth.

II. Assumption: *The total stress demand can be used to estimate the effective stress demand.* From Fig. 8a), the number of equivalent cycles from the ESA was considerably less than that from NTLSA and SBM, therefore this assumption led to an overprediction.

III. Assumption: *An irregular loading can be converted to an equivalent uniform loading using the Palmer-Miner cumulative damage hypothesis and the liquefaction resistance curve as the amplitude equivalence function.* From Fig. 13a), the behaviour of the PM4Sand model at several depths versus the equivalent number of stress cycles is plotted against the assumption adopted in the SBM using the [31] relationship. Remarkably the irregular loading requires about three times more equivalent loading cycles to reach liquefaction than what was predicted. While the PM4Sand model is only a

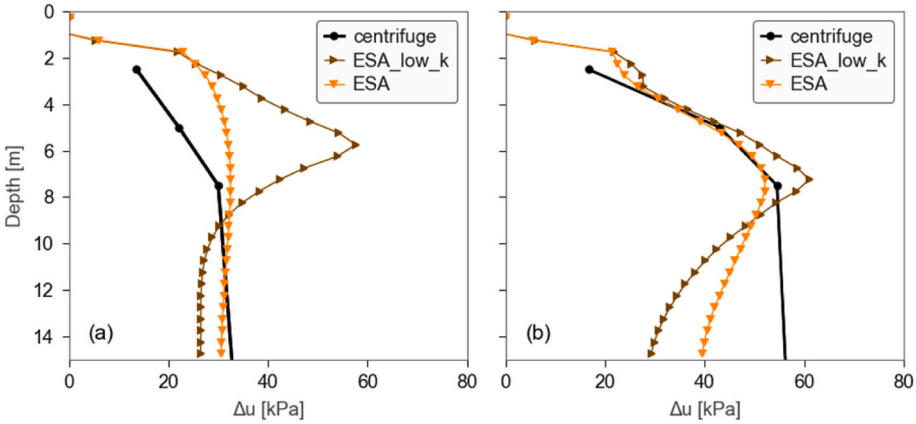

Fig. 10. Comparison of the pore pressure (Δu) profile with depth at 24 s estimated by the numerical analysis with two different permeability values together with the centrifuge tests results: a) data from test 10 indicated in Table 2; b) data from test 11 indicated in Table 2.

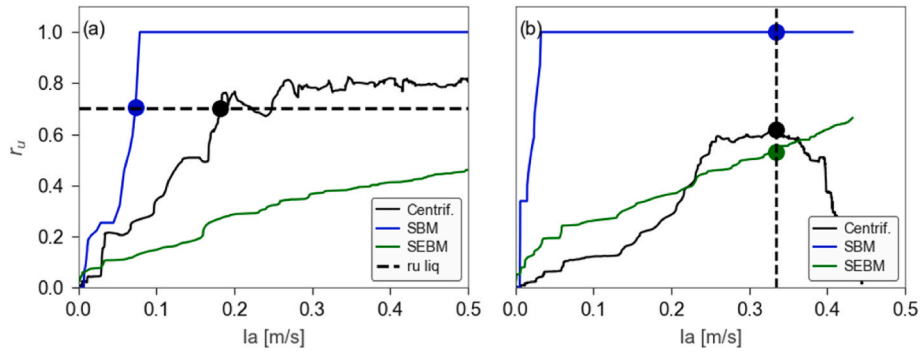

Fig. 11. Example of Category A sensors ($r_u \geq 0.7$) (a) and Category B sensors ($r_u < 0.7$).

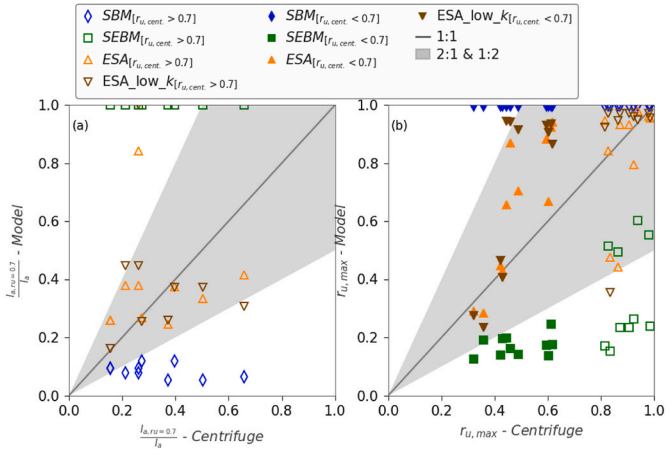

Fig. 12. Comparison between simplified methods, centrifuge tests and numerical analysis in terms of: a) Arias Intensity, for sensors where $r_u \geq 0.7$ in the centrifuge tests, b) for $r_{u,max}$ for sensors where $r_u < 0.7$ in the centrifuge tests.

surrogate for the behaviour of real soil, the strong match between the centrifuge results and ESA results suggests that the equivalent loading assumption is causing a significant overprediction in the development of pore pressure.

IV. Assumption: *The development of pore pressure assumes undrained conditions.* As demonstrated in Fig. 10 the influence drainage can both increase and decrease the level of pore pressure, typically reducing it in regions of higher seismic demand and increasing it in regions of lower demand. The smoothing out of pore pressure caused by drainage is not accounted for in the SBM. Furthermore near a free-draining surface the pore water can escape reducing pore pressure in the surrounding soil.

Overall the overprediction caused by both the total stress assumption (II) and equivalent loading (III) led to a significant overprediction in pore pressure compared to the centrifuge results, even though significant drainage occurred which generally reduced pore pressure in the centrifuge compared to an undrained assumption. The improvement in demand from total stress through some accounting of energy loss due to soil softening may improve estimates from (II). Meanwhile, research by Ref. [14] provides an alternative to the Palmer-Miner hypothesis for computing equivalent cycles, potentially overcoming the significant overprediction observed in (III).

8.2. *Evaluation of assumptions of the strain energy based method*

The different assumptions of the simplified strain energy based method as outlined below were evaluated based on the results of test 11 using Figs. 8b), 9 and 13b):

I. Assumption: *The total stress cyclic stress at depth can be computed using the nodal surface energy spectrum with corrections for energy loss (damping) and changes in soil stiffness.* From Fig. 8b), a comparison of the NCASE demand from SEBM versus that from NLTSA, it is clear that the demand is underestimated in the top 6 m and overpredicted in the lower part of the deposit. This difference is largely attributed to the variation in shear stiffness of the soil that [12] recognise as not being properly addressed within the procedure.

II. Assumption: *The total stress demand is equivalent to the effective stress demand.* From Fig. 8b), the NLTSA clearly shows significantly lower demand versus the ESA results in the top 6 m and the

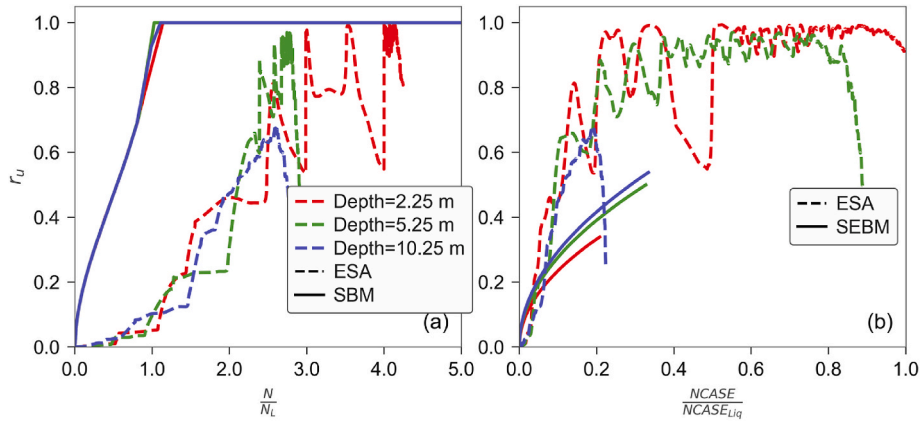

Fig. 13. Analysis of pore pressure with N_L/N (a) and NCASE (b) estimated by the simplified methods with the numerical analysis (ESA).

opposite for the lower part of the deposit. This leads to a further overprediction and underprediction of demand at different depths.

III. Assumption: *The build up of pore pressure is independent of the amplitude of loading.* This assumption appeared to be consistent with observations from the element tests in Fig. 3. Furthermore, the FLAC element tests were also examined in Fig. 14, where pore pressure appears to be independent of load amplitude. However, Fig. 14 highlights that FLAC element tests build up pore pressure more rapidly than the prediction function that was calibrated to the experimental test – detailed examination found that this was due to the higher effective stiffness for a given r_u compared to the experimental data. This suggests that a calibration procedure that targets not only the cyclic resistance curve, but also the rate of change of effective stiffness may improve consistency between the energy based prediction and the results from FLAC. Furthermore, the strain energy based capacity obtained from the element tests may not directly correspond to the capacity under free-field seismic loading as the capacity relied on a conversion from triaxial loading to equivalent direct simple shear loading.

IV. Assumption: *The development of pore pressure assumes undrained conditions.* The conclusions here are the same as for the SBM.

Overall the underprediction in demand from assumptions (I) and (II) resulted in an underprediction of pore pressure, while the inconsistency in the calibration suggests that the $NCASE_{liq}$ may have been too high, or the effective stiffness in the FLAC analyses may have been too high, and improved calibration focusing on strain development as well as matching the liquefaction resistance curve may yield improved results.

The SEBM shows promising results but it should be noted that at present there is not a way to estimate SEBM capacity ($NCASE_{liq}$) from in situ data compared to the widely established procedures for the SBM. Furthermore, there is no ground motion prediction equation available to obtain the nodal surface energy spectrum needed for predicting demand from a future event.

9. Conclusions

Earthquake induced structural damage is very dependent on both the extent of and timing of liquefaction. The increase in pore pressure (even leading only to partial liquefaction) decreases the stiffness properties of the soil, affecting the seismic response of the soil and consequently the seismic excitation arriving at the surface that shakes the structures. Therefore, it is very important to develop methods that may improve the estimate of the seismic energy arriving at the surface in liquefiable soil.

In this work, two simplified methods for estimating pore pressure development are evaluated against a series of centrifuge tests performed at ISMGEO, Italy. One of the methods was based on the equivalent cyclic stress following the ideas of [13] and others (e.g., Ref. [9]). The other method was based on the accumulated strain energy as proposed by Ref. [12]. As most centrifuge tests were performed on Ticino Sand, the cyclic resistance of this sand was evaluated by the interpretation of cyclic triaxial tests performed by Ref. [33]. In addition, 1D numerical simulations of the centrifuge tests were performed using the PM4sand model, where the input parameters were calibrated with the laboratory tests, showing a good agreement between the results.

Although a limited number of ground motions and soil conditions were used in the study, the bias of the simplified methods in comparison to the centrifuge data and numerical analysis were discussed with reference to the assumptions of each method. The stress based method tended to overpredict the excess pore pressure compared to the centrifuge recordings. Meanwhile the strain energy based method tended to underpredict pore pressure. In the stress based method the issues were attributed to the difficultly of estimating demand in a liquefying deposit, the conversion of irregular loading to uniform loading, and pore water flow not being considered in the simplified model. For the strain energy based method, the estimation of the demand did not accurately account for the variation in soil stiffness or change in demand due to liquefaction, as well as issues with capacity related to calibration and converting triaxial test data to equivalent simple shear data may have resulted in biases.

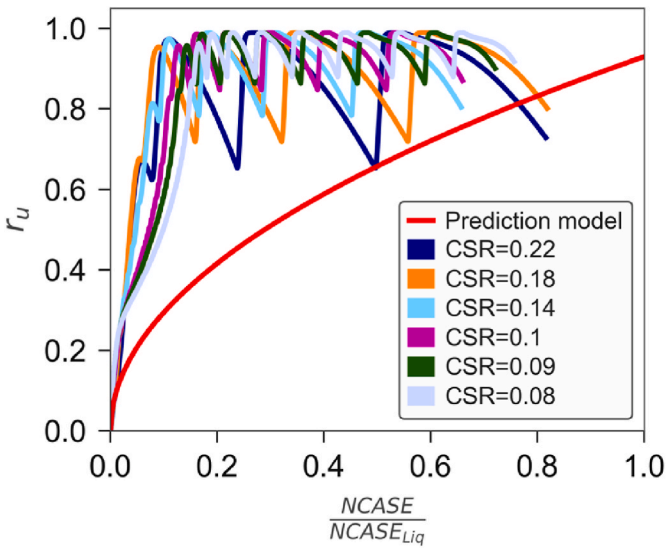

Fig. 14. Analysis of pore pressure with $NCASE/NCASE_{liq}$ from FLAC element tests.

CRediT authorship contribution statement

Sara Rios: Writing – original draft, Investigation, Visualization, Formal analysis. **Maxim Millen:** Conceptualization, Methodology, Investigation, Software, Writing – review & editing. **Julieth Quintero:** Visualization, Validation, Formal analysis. **António Viana da Fonseca:** Resources, Project administration, Funding acquisition.

Declaration of competing interest

The authors declare that they have no known competing financial interests or personal relationships that could have appeared to influence the work reported in this paper.

Acknowledgments

LIQUEFACT project (Assessment and mitigation of liquefaction potential across Europe: a holistic approach to protect structures/infrastructures for improved resilience to earthquake-induced liquefaction disasters) has received funding from the European Union's Horizon 2020 research and innovation programme under grant agreement GAP-700748. This work was also financially supported by: Base Funding - UIDB/04708/2020 of the CONSTRUCT - Instituto de I&D em Estruturas e Construções - funded by national funds through the FCT/MCTES (PIDDAC). The third author acknowledges the support of Portuguese Foundation for Science and Technology (FCT) through the grant SFRH/BD/143817/2019.

The authors would like to acknowledge Professor Vincenzo Fioravante and Doctor Daniela Giretti for supplying the Ticino sand cyclic triaxial test results and the geotechnical ISMGEO centrifuge monitoring data. This is due to Ing. Sergio Airoldi skills and competence in conducting the experimental work in the centrifuge facility.

References

[1] Bray JD, Sancio RB, Durgunoglu T, Onalp A, Youd TL, Stewart JP, Seed RB, Cetin OK, Bol E, Baturay MB, Christensen C, Karadayilar T. Subsurface

characterization at ground failure sites in Adapazari, Turkey. J Geotech Geoenviron Eng 2004;130(7):673–85.
[2] Cubrinovski M, Bray J, Taylor M, Giorgini S, Bradley B, Wotherspoon L, Zupan J. Soil liquefaction effects in the central business district during the February 2011 Christchurch earthquake. Seismol Res Lett 2011;82(6):893–904.
[3] Bray JD, Markham CS, Cubrinovski M. Liquefaction assessments at shallow foundation building sites in the Central Business District of Christchurch, New Zealand. Soil Dynam Earthq Eng 2017;92(10):153–64. https://doi.org/10.1016/j.soildyn.2016.09.049.
[4] Yamaguchi Y, Kondo M, Kobori T. Safety inspections and seismic behaviour of embankment dams during the 2011 off the Pacific Coast of Tohoku earthquake. Soils Found 2012;52(5):945–55.
[5] Kramer SL, Sideras SS, Greenfield MW. The timing of liquefaction and its utility in liquefaction hazard evaluation. Soil Dynam Earthq Eng 2016;91:133–46.
[6] Özener PT, Greenfield MW, Sideras SS, Kramer SL. Identification of time of liquefaction triggering. Soil Dynam Earthq Eng 2020;128. 105895–15.
[7] Karatzia X, Mylonakis G, Bouckovalas G. Seismic isolation of surface foundations exploiting the properties of natural liquefiable soil. Soil Dynam Earthq Eng 2019;121:233–51. https://doi.org/10.1016/j.soildyn.2019.03.009.
[8] Kramer S, Hartvigsen AJ, Sideras SS, Ozener PT. Site response modelling in liquefiable soil deposits. In: 4th IASPEI - effects of surface geology on seismic motion; 2011. p. 1–12.
[9] Boulanger RW, Idriss IM. CPT and SPT based liquefaction triggering procedures. Retrieved from. Davis: Center for Geotechnical Modelling, University of California; 2014. p. 134. Report No. UCD/CGM-14/01, http://nees.ucdavis.edu/publications/Boulanger_Idriss_CPT_and_SPT_Liq_triggering_CGM-14-01_2014.pdf.
[10] Robertson PK, Wride CE. Evaluating cyclic liquefaction potential using the cone penetration test. Can Geotech J 1998;35(3):442–59. https://doi.org/10.1139/t98-017.
[11] Rios S, Viana da Fonseca A, Millen M. Evaluation of pore pressure prediction models from centrifuge tests in liquefiable soils. In: Proceedings of the 20th international conference on soil mechanics and geotechnical engineering, Sydney; 2021.
[12] Millen M, Rios S, Quintero J, Viana da Fonseca A. Prediction of time of liquefaction using kinetic and strain energy. Soil Dynam Earthq Eng 2020:105898. https://doi.org/10.1016/j.soildyn.2019.105898. 128.
[13] Seed H, Idriss I, Makdidi F, Nanerjee N. Representation of irregular stress time histories by equivalent uniform stress series in liquefaction analyses Report No. EERC 75–29. Earthquake Engineering Research Center. University of California Berkeley; 1975.
[14] Green RA, Terri GA. Number of equivalent cycles concept for liquefaction evaluations—revisited. J Geotech Geoenviron Eng 2005;131(4):477–88. https://doi.org/10.1061/(ASCE)1090-0241(2005)131:4(477).
[15] Dobry R, Pierce W, Dyvik R, Thomas G, Ladd R. Pore pressure model for cyclic straining of sand. Troy: Civil Engineering Department, Rensselaer Polytechnic Insti-Tute; 1985.
[16] Ivšić T. A model for presentation of seismic pore water pressures. Soil Dynam Earthq Eng 2006;26(2–4):191–9. https://doi.org/10.1016/j.soildyn.2004.11.025.
[17] Finn W, Bhatia S. Prediction of seismic porewater pressures. In: Proceedings of the 10th international conference on soil mechanics and foundation engineering; 1982. p. 201–6.
[18] Park T, Park D, Ahn JK. Pore pressure model based on accumulated stress. Bull Earthq Eng 2015;13(7):1913–26. https://doi.org/10.1007/s10518-014-9702-1.
[19] Chiaradonna A, Tropeano G, d'Onofrio A, Silvestri F. Development of a simplified model for pore water pressure build-up induced by cyclic loading. Bull Earthq Eng 2018;16(9):3627–52. https://doi.org/10.1007/s10518-018-0354-4.
[20] Nemat-Nasser S, Shokooh A. A unified approach to densification and liquefaction of cohesionless sand in cyclic shearing. Can Geotech J 1979;16(4):659–78. https://doi.org/10.1139/t79-076.
[21] Davis R, Berril J. Energy dissipation and seismic liquefaction in sands. Earthq Eng Struct Dynam 1982;10(1):59–68. https://doi.org/10.1002/eqe.4290100105.
[22] Green RA, Mitchell JK, Polito CP. An energy-based excess pore pressure generation model for cohesionless soils. In: Proceeding of the John Booker Memorial Symposium; 2000. p. 1–9.
[23] Kokusho T. Liquefaction potential evaluations: energy-based method versus stress-based method. Can Geotech J 2013;50(10):1088–99. https://doi.org/10.1139/cgj-2012-0456.
[24] Kokusho T. Energy-based liquefaction evaluation for induced strain and surface settlement – evaluation steps and case studies. Soil Dynam Earthq Eng 2021;143:106552. https://doi.org/10.1016/j.soildyn.2020.106552.
[25] Roscoe KH, Schofield AN, Thurairajah A. Yielding of clays in states wetter than critical. Geotechnique 1963;13(3):211–40.
[26] Cubrinovski M, Ishihara K. Modelling of sand behaviour based on state concept. Soils Found 1998;38(3):115–27. https://doi.org/10.3208/sandf.38.3_115.
[27] Azeiteiro R, Coelho P, Taborda D, Grazina J. Energy-based evaluation of liquefaction potential under non-uniform cyclic loading. Soil Dynam Earthq Eng 2017;92:650–65. https://doi.org/10.1016/j.soildyn.2016.11.005.
[28] Ntritsos N, Cubrinovski M. A CPT-based effective stress analysis procedure for liquefaction assessment. Soil Dynam Earthq Eng 2020;131:106063. https://doi.org/10.1016/j.soildyn.2020.106063.
[29] Idriss IM. An update to the Seed-Idriss simplified procedure for evaluating liquefaction potential. In: TRB workshop on New approaches to liquefaction publication No. FHWARD- 99-165. Federal Highway Administration; 1999.
[30] Boulanger RW, Idriss IM. CPT-based liquefaction triggering procedure. J Geotech Geoenviron Eng 2016;142(2):4015065. https://doi.org/10.1061/(ASCE)GT.1943-5606.0001388.
[31] Booker JR, Rahman MS, Seed HB. GADFLEA— a computer program for the analysis of pore pressure generation and dissipation during cyclic or earthquake loading. Rep. No. EERC 1976. 76-24.
[32] Polito CP, Green RA, Lee J. Pore pressure generation models for sands and silty soils subjected to cyclic loading. J Geotech Geoenviron Eng 2008;134(10):1490–500. https://doi.org/10.1061/(ASCE)1090-0241(2008)134:10(1490).
[33] Fioravante V, Giretti D. Unidirectional cyclic resistance of Ticino and Toyoura sands from centrifuge cone penetration tests. Acta Geotech 2016;11:953–68. https://doi.org/10.1007/s11440-015-0419-3.
[34] Bilotta E, Chiaradonna A, Fasano G, Flora A, Mele L, Nappa V, Lirer S, Fioravante V. Experimental evidences of the effectiveness of some liquefaction mitigation measures. Zenodo 2019. https://doi.org/10.5281/zenodo.3463346.
[35] Ozcebe AG, Giretti D, Bozzoni F, Fioravante V, Lai C. Centrifuge and numerical modelling of earthquake-induced soil liquefaction under free-field conditions and by considering soil–structure interaction. Bull Earthq Eng 2021;19:47–75. https://doi.org/10.1007/s10518-020-00972-3. 2021.
[36] Karg C, Haegeman W. Elasto-plastic long-term behaviour of granular soils: experimental investigation. Soil Dynam Earthq Eng 2009;29:155–72. https://doi.org/10.1016/J.SOILDYN.2008.01.001.
[37] Baldi G, Belloni G, Maggioni W. The ISMES geotechnical centrifuge. In: Corté JF, editor. Centrifuge 88, Paris. Rotterdam: Balkema; 1988. p. 45–8.
[38] Airoldi S, Fioravante V, Giretti D, Moglie J. Deliverable D 4.2 - Report on validation of retrofitting techniques from small scale models. LIQUEFACT Project, Horizon 2020 European Union funding for Research & Innovation, GA. Nº; 2018, 700748. www.liquefact.eu.
[39] Fioravante V, Giretti D, Airoldi S, Moglie J. Effects of seismic input, fine crust and existing structure on liquefaction from centrifuge model tests. Bull Earthq Eng 2021;19(10):3807–33. https://doi.org/10.1007/s10518-021-01139-4.
[40] Fioravante V, Jamiolkowski M. In: Physical modelling of piled rafts. Soil structure interaction: calculation methods and engineering practice. International geotechnical conference. Saint Petersburg. May 2005; 2005. p. 89–95.
[41] Flora A, Bilotta E, Chiaradonna A, Lirer S, Mele L, Pingue L. A field trial to test the efficiency of induced partial saturation and horizontal drains to mitigate the susceptibility of soils to liquefaction. Bull Earthq Eng 2021;19(10):3835–64. https://doi.org/10.1007/s10518-020-00914-z.
[42] Airoldi S, Fioravante V, Giretti D, Moglie J. Validation of liquefaction retrofitting techniques from geotechnical centrifuge small scale models [Data set]. Zenodo; 2018. https://doi.org/10.5281/zenodo.1281598.
[43] Kayen RE, Mitchell JK. Assessment of liquefaction potential during earthquake by Arias Intensity. J Geotech Geoenviron Eng 1997;123(12):1162–74.
[44] Campbell KW, Bozorgnia YA. Comparison of ground motion prediction equations for Arias intensity and cumulative absolute velocity developed using a consistent database and functional form. Earthq Spectra 2012;28(3):931–41. https://doi.org/10.1193/1.4000067.
[45] Itasca Consulting Group, Inc. FLAC — Fast Lagrangian Analysis of Continua, Ver. 8.0. Minneapolis: Itasca; 2016.
[46] Fasano G, Valeria N, Özcebe AG, Bilotta E. Numerical modelling of the effect of horizontal drains in centrifuge tests on soil-structure interaction in liquefiable soils. Bull Earthq Eng 2021;19(10):3895–931. https://doi.org/10.1007/s10518-021-01084.
[47] Boulanger R, Ziotopoulou K. PM4Sand (Version 3.1): a sand plasticity model for earthquake engineering applications. Davis: Center for Geotechnical Modelling, Department of Civil and Environmental Engineering College of Engineering, University of California; 2017. Report No. UCD/CGM-17/01. Technical report.
[48] Dafalias Y, Manzari M. Simple plasticity sand model accounting for fabric change effects. J Eng Mech 2004;130(6):622–34.
[49] Vardanega PJ, Bolton MD. Stiffness of clays and silts: normalizing shear modulus and shear strain. J Geotech Geoenviron Eng 2013;139(9):1575–89. https://doi.org/10.1061/(ASCE)GT.1943-5606.0000887.
[50] Rios S, Millen M, Viana da Fonseca A, Santos P, Mudanò G. Validação de modelos simplificados de previsão do tempo de liquefação através de ensaios de centrifugadora. Revista Geotecnia 2020;148:31–54. https://doi.org/10.24849/j.geot.2020.148.03 [in portuguese)].